



HAL
open science

Experimental disc heat flux identification on a reduced scale braking system using the inverse heat conduction method

Damien Méresse, Souad Harmand, M. Siroux, Michel Watremez, Laurent Dubar

► To cite this version:

Damien Méresse, Souad Harmand, M. Siroux, Michel Watremez, Laurent Dubar. Experimental disc heat flux identification on a reduced scale braking system using the inverse heat conduction method. Applied Thermal Engineering, 2012, 48, pp.202-210. 10.1016/j.applthermaleng.2012.04.033 . hal-02367753

HAL Id: hal-02367753

<https://uphf.hal.science/hal-02367753>

Submitted on 18 Nov 2019

HAL is a multi-disciplinary open access archive for the deposit and dissemination of scientific research documents, whether they are published or not. The documents may come from teaching and research institutions in France or abroad, or from public or private research centers.

L'archive ouverte pluridisciplinaire **HAL**, est destinée au dépôt et à la diffusion de documents scientifiques de niveau recherche, publiés ou non, émanant des établissements d'enseignement et de recherche français ou étrangers, des laboratoires publics ou privés.

Experimental disc heat flux identification on a reduced scale braking system using the inverse heat conduction method

D.Meresse^{a,b}, S.Harmand^{a,b,*}, M.Siroux^c, M.Watremez^{a,b}, L.Dubar^{a,b}

^aUniv Lille Nord de France, F-59000 Lille, France

^bUVHC, TEMPO EA 4542, F-59313 Valenciennes, France

^cINSA, LGECO EA 3938, F-67084 Strasbourg, France

Abstract

This work focuses on the local heat fluxes on a disc during braking conditions. The generated heat and the temperature field are identified using an inverse heat conduction method coupled to temperature measurements inside the disc. Function specification is used to estimate the boundary conditions in the model without any prior information on the flux intensity and the evolution regarding the time and the position on the sliding surface. Disc heat flux identifications are performed for different braking conditions (sliding speed and normal pressure) on a high-speed tribometer. The temperature values are obtained using a telemetry system that allows inductive data transfer. The influence of the braking conditions on the heat repartition and the surface temperature is discussed.

Keywords: Inverse method, Telemetry measurement, Braking conditions, High Speed Tribometer

1. Introduction

In automotive brake linings, the friction materials are used to rapidly dissipate the kinetic energy on small surfaces. The pads and the disc are then subjected to severe thermal and mechanical stresses. The tribological and wear behaviours are affected by the temperature elevation in the contact zone [1]. A loss of braking efficiency is observed for organic brake pads with this temperature elevation. This loss of efficiency is caused by phenolic resin degradation above 300°C

*Corresponding author

**Principal corresponding author

Email address: souad.harmand@univ-valenciennes.fr (S.Harmand)

[2], which varies with the chemical formulation. Efforts are aimed at finding some way to cool the disc [3] [4] [5] and limit the temperature elevation. The thermal conditions are essential for better understanding the physical phenomena occurring at the interface. The heat partition is generally defined by the parameter α , that defines the part of the heat dissipated on the disc side. Due to contact zone asperities and the dynamic effects, differences between the disc and pad surface temperatures have been observed. It is also necessary to define a contact thermal resistance R_c [6] depending on the sliding speed, materials, and wear debris.

Some particular temperature fields have been observed using thermography on the disc contact surface. Anderson has named and classified them as hot spots [7]. The temperature can locally achieve values greater than 1200°C on asperities. This phenomenon is defined by Blok [8] as the flash temperature, and Greenwood has suggested a way to evaluate their values [9]. Macroscopic spots originate in thermoelastic instabilities [10]. These spots preferentially appear in cases of severe braking conditions [11]. Dufrenoy [12] has highlighted that this heat localisation is responsible for disc damage because the thermal gradients induce mechanical stresses.

Unfortunately, the emissivity of the disc changes with the temperature and surface roughness during braking. To accurately measure the surface temperature, emissivity cartography is needed, as identified in a previous work [13]. Thevenet [14] has developed a specific two-colour pyrometer to simultaneously measure the emissivity and surface temperature below 200°C. This is possible by assuming that the emissivity value does not vary with the wavelength and that the disc can be considered as a grey body in the wavelength range. The two-colour pyrometer was then used by Kasem [15] to obtain corrected surface temperature values by coupling it with an infrared camera. Additionally, Siroux [16] has measured the local disc-pin interface temperature through a calcium fluoride window embedded at the pin side.

At the same time, analytical and numerical models have been developed to estimate the heat repartition in the antagonist parts and to predict the temperatures fields. Siroux has identified the temperature field in a disc subject to periodic sliding contact using a model based on the Fourier transform algorithm [17]. Laraqi has studied the 3D disc temperature field in steady states [18], i.e., when the loss by convective heat transfer is balanced by the heat generated during a rotation.

This analytical model highlights the influence of the disc rotary speed on the heat trail shape. In the case of transient problems, numerical resolutions are more suitable than analytic identifications. The inverse heat conduction method can be used to calculate the thermal conditions and the boundary conditions of the numerical model. As the resolution is sequential, this algorithm is efficient in identifying the heat fluxes without prior information on the evolution in the time. Yang has demonstrated the ability to calculate the boundary conditions on a brake disc by simulating experimental data using a direct model [19]. He showed that it is necessary to take care in choosing the sensor locations to obtain accurate results using the inverse method.

In this work, heat generation is studied using a reduced scale pin-on-disc tribometer: the High Speed Tribometer. This experimental setup has been developed to study the heat generation in severe sliding conditions. The disc and pin dimensions have been chosen to keep the thermal conditions close to the full-scale heat repartition. Temperature measurements are performed inside the moving part using K-type thermocouples and a telemetry system. The heat fluxes on the disc friction ring are calculated using the function specification method largely developed by Beck [20]. This enables the evaluation of the repartition along the disc radial direction using an axisymmetric model. In this study, experimental tests are performed under a constant mean normal pressure and sliding speed conditions with self-made materials. The pin is made of pure phenolic resin that is used as a matrix in organic brake pads, and the disc is made of low carbon steel. The braking conditions' influence on the heat distribution and intensity is discussed.

2. Inverse heat conduction method

2.1. Disc model

The heat conduction equation (Eq.1) is solved in a two-dimensional axisymmetric configuration. This configuration has been chosen based on Laraqi's work [18] on the 3D temperature field in a braking disc. According to the convective heat loss during one rotation and the temperature gradient along the angular direction, heat flux identification can be performed on the (r,z) axes. Additionally, solving the inverse problem in a three dimensional model would need a large

number of sensors. The holes added to insert the thermocouples in the disc would disturb the temperature field considerably [21] and would give poor identification results.

$$\frac{1}{a_d} \frac{\partial T(r, z, t)}{\partial t} = \frac{1}{r} \frac{\partial}{\partial r} \left(r \frac{\partial T(r, z, t)}{\partial r} \right) + \left(\frac{\partial^2 T(r, z, t)}{\partial z^2} \right) \quad (1)$$

The direct problem is illustrated in Figure 1. The disc and pin dimensions have been chosen according to the reduced scale rule (detailed in 3.2). The disc is 100 mm in diameter and 10 mm in thickness. The friction ring defines the boundary where the generated heat fluxes are dissipated, i.e., the unknown boundary conditions. The disc is rubbed between $R_{fint}=24$ mm and $R_{fext}=48$ mm.

Insulation boundary conditions are imposed on the disc surfaces that are in contact with the attachments (Eq.2). The insulation conditions are applied on the disc's internal radius at $R_{int}=8$ mm and on part of the back face through $R_{insu}=22$ mm. As described in the experimental part, a material with low thermal conductivity is used to limit the external thermal conductive transfers as soon as possible. The other disc surfaces without solid contact are considered to be cooled by air flow. The convective heat transfers (Eq.3) are modelled using convective coefficients depending on the disc's rotary speed and the radial position. These coefficients are calculated using the correlation (Eq.4) from Siroux [22]. For a Reynolds number value $Re < 1.8 \times 10^5$, the air flow on the disc surface is laminar and the convective coefficient only depends on the rotary speed. Above 2.8×10^5 , the air flow is turbulent and the convective coefficient depends on the air's thermal conductivity k_{air} , the radial position r and the Reynolds number. For intermediate Re values, the h values are calculated using a linear interpolation.

$$\left\{ \begin{array}{l} -k_d \frac{\partial T(r, z, t)}{\partial r} \Big|_{z, r=R_{int}} = 0 \\ -k_d \frac{\partial T(r, z, t)}{\partial z} \Big|_{z=z_d, r < R_{finsu}} = 0 \end{array} \right. \quad (2)$$

$$\left\{ \begin{array}{l} -k_d \frac{\partial T(r, z, t)}{\partial r} \Big|_{z, r=R_{ext}} = h_{R_{ext}}(T_\infty - T(r, z, t)) \\ -k_d \frac{\partial T(r, z, t)}{\partial z} \Big|_{z=0, r < R_{fint}} = h(r)(T_\infty - T(r, z, t)) \\ -k_d \frac{\partial T(r, z, t)}{\partial z} \Big|_{z=0, r > R_{fext}} = h(r)(T_\infty - T(r, z, t)) \\ -k_d \frac{\partial T(r, z, t)}{\partial z} \Big|_{z=0, r > R_{insu}} = h(r)(T_\infty - T(r, z, t)) \end{array} \right. \quad (3)$$

$$\left\{ \begin{array}{l} Re = \frac{\omega r^2}{\nu_{air}} \\ h = 2.48 \sqrt{\omega} \quad (Re < 1.8 * 10^5) \\ h = 0.0194 k_{air} \frac{Re^{0.8}}{r} \quad (Re > 2.8 * 10^5) \end{array} \right. \quad (4)$$

On the friction ring, it is necessary to consider convective heat transfers as each location on the surface is successively rubbing and moving out of the contact zone. As described by (Eq.5), the convective coefficients are here weighted by the free-surface angular ratio $S_{ratio}(r)$, which is defined by the friction sliding angle divided by 2π .

$$-k_d \frac{\partial T(t)}{\partial z} \Big|_{z=0, R_{fint} < r < R_{fext}} = \varphi(r, t) * (1 - S_{ratio}(r)) + \dots \\ S_{ratio}(r)h(r)(T_\infty - T(r, z = 0, t)) \quad (5)$$

This parameter evolution along the radial position is plotted in Figure 2. Due to the pin on disc configuration, the S_{ratio} value changes with the radial position on the friction ring. In our experimental case, the pin is 24 mm in diameter and the mean friction radius on the disc is 36 mm.

The direct problem is solved using a finite difference method with an implicit resolution. After a study to optimise the mesh size, we have chosen to discretise the disc with $\delta r=1$ mm and $\delta z=1$ mm. Its thermal properties come from [23] and are considered constant. Over the experimental temperature range (20-400°C), the thermal conductivity and the specific heat variations are lower than 5%. The constant values used are listed in Table 1.

k_d	Cp_d	ρ_d
$W.m^{-1}.K^{-1}$	$J.kg^{-1}.K^{-1}$	$kg.m^{-3}$
52	480	7850

Table 1: Disc thermal properties

2.2. Function specification method

The function specification method is a very efficient inverse technique to determine the transient behaviour in thermal problems. Indeed, this allows to identify thermal properties or boundary conditions [24] without any knowledge about their shape and their dependence regarding the model parameters. The algorithm is based on incremental error estimations of the unknown boundary conditions that minimise the difference between calculated and experimental temperature values. The difference function J is defined by the equation (Eq.6).

$$J(\varphi(r)) = \sum_{i=1}^N \left[\sum_{j=1}^r (Y_i^{t+j*\delta t} - T_i^{t+j*\delta t})^2 \right] \quad (6)$$

For each time increment δt , an assumption on boundary values is performed for several future time steps. In many studies [25], the values are chosen to be constant as in our case. The direct problem is then solved to obtain the temperature field over the whole domain for several future time increments. The numerical values obtained at the sensors locations are then compared to the experimental data. The errors associated with the boundary conditions, due to the constant-value assumption, are calculated to minimise the temperature quadratic differences defined by the J function. Finally, a direct resolution is performed with the corrected heat fluxes for one future time step. This procedure is repeated until the end of the test duration.

As described above, the temperature error and the boundary condition estimations have to be performed on several future time increments. Introducing a temporal stabilisation is necessary when using the inverse problem. As the experimental data always contain some noise, strong disturbances are induced in the calculated heat fluxes. In addition to smoothing the temperature data, solving the inverse problem for future time increments allows for avoiding calculation divergence. However, this technique induces a bias in the estimated values. The number of future time steps

nft has to be chosen to get a good balance between stability and smoothing.

The time increment δt and the number of future time steps nft are chosen according to the sensitivity coefficient X . This is defined by the temperature variation at the measurement location for a unitary heat flux variation on the friction ring (eq 7).

$$X_{iii}^{t+j\delta t} = \frac{\partial T_i^{t+j\delta t}}{\partial \varphi_{ii}^{t+j\delta t}} \quad (7)$$

A sensitivity analysis is illustrated in the Figure 3. For a heat flux variation imposed on the disc surface for $r=36$ mm at $t=0$, the temperature variations 1 mm under this surface are plotted for different radial positions. The thickness position is imposed by the experimental conditions. The sensitivity reaches a maximum value after 0.05 s at the same radial position. For the neighbouring locations ($r=34$ mm and $r=38$ mm), more time is needed to achieve the greatest temperature elevation (approximately 0.13 s). The time required rapidly grows with the distance from the heated surface. A sensor located 4 mm from the heat radial position needs 0.34 s to achieve the highest temperature elevation. Regarding these considerations, the inverse problem is solved with a time increment of $\delta t=0.05$ s. The choice of the number of future time steps nft is linked to the sensor number and locations.

2.3. Choice of the sensors locations and of the number of future time steps nft

The sensors' locations have to be well chosen to obtain good estimations using the function specification method. In multi-dimensional problems, using an inverse technique requires that each unknown heat flux is similarly represented, i.e., the sensors' sensitivities are equivalent for all the boundary positions. The rate of representation τ (eq.8) is a practical tool to determine the number of thermocouples needed, the locations to insert them and the number of future time steps. This parameter is calculated with the sensitivity coefficients X (Eq.7). The rate of representation allows rapidly testing several configurations without solving the entire inverse problem. The choice of the sensors locations and the number of future time steps nft are linked and have to be determined together. The locations are acceptable as long as none of the rate of heat fluxes

represented are less than 75% of the most well-represented unknown.

$$\tau_{ii}^r = \sum_{i=1}^N X_{i|ii}^r \quad (8)$$

In the Figure 4, the representative rate for 4 different conditions, among many tested, are plotted. In all cases, one sensor is assumed to be at the minimum friction radius $R_{fint}=24$ mm, and another sensor is assumed at the maximum friction radius $R_{fext}=48$ mm. The remainder are regularly spread between the two extreme locations. Due to the hole machining constraints, the thickness position is fixed at 1 mm from the rubbing surface. Cases with five and seven thermocouples sensors are illustrated here. Considering our experimental possibilities, the number of thermocouples is restricted to eight. Regarding cases with five sensors, we can see that there is a lack of information for locations 3 mm from the sensors in the radial direction. With $nft = 7$, the normalised representative rate is lower than 45%. Choosing $nft = 12$ allows for an improvement in the heat flux representation, but some rates are lower than 55%, and the temporal stabilisation will induce an important error in the estimation. With 7 sensors, the minimum normalised rate is greater than 63% for $nft = 5$ and reaches the minimum value of 75% for $nft = 7$. This last configuration with seven sensors and $nft = 7$ is selected because it offers a good balance between the heat fluxes representation and the temporal stabilisation. As shown in Figure 5, the sensors are spaced every 4mm along the radial direction from $R_{fint}=24$ mm to $R_{fext}=48$ mm on the experimental set-up and are distributed along the angular direction (45°). The angular repartition is chosen to limit the temperature field disturbances caused by the holes.

2.4. Spatial stabilisation

In the case of the multidimensional problems, the number of unknown heat fluxes M generally becomes more important than the number of sensors N . As described above, the experimenter has to reduce the thermocouple number to avoid a thermal field perturbation. There are some difficulties in solving the inverse problem. In this case, many solutions for the heat flux distribution will exist, which allows minimizing the numerical-experimental temperature difference. It is then necessary to apply a spatial stabilisation. A term is added in (Eq.6) to avoid non-physical heat value fluctuations for neighbouring positions. In the modified equation (Eq.9), the parameter β

allows for the reduction of the spatial heat flux variations from one interpolation point to another. As in the temporal stabilisation, the chosen value of β has to be made considering a balance between avoiding spatial fluctuations and introducing a bias. According to Blanc [26], an efficient value of β can be estimated while considering the sensitivity coefficient X without solving the entire inverse problem.

$$J_{\beta} = J + \beta \sum_{ii=1}^{M-1} (\varphi_{ii-1}^{t+\delta t} - 2\varphi_{ii}^{t+\delta t} + \varphi_{ii+1}^{t+\delta t}) \quad (9)$$

2.5. Numerical validation

A numerical validation of the inverse method is performed using the source file method as used by Yang [19]. This allows for the confirmation of the choice of the number of future time steps nft and of the sensors locations and allows for choosing a consistent value for the spatial stabilisation parameter β . The temperature field is calculated in the whole domain for the imposed heat fluxes on the friction ring. The temperature data are then extracted from the numerical results and white noise (0.05°C) is added to simulate experimental data coming from the sensors locations. The function specification method is then applied to find the imposed boundary conditions.

The imposed heat fluxes are chosen to obtain conditions close to the values found in the experimental tests. The heat generated is calculated using (Eq.10) for the following values : $\alpha = 0.995$, $P = 1 \text{ MPa}$, $v = 7.5 \text{ m.s}^{-1}$ and $\mu = 0.5$. The disc is also heated for 30 s ($10 \rightarrow 40 \text{ s}$) with a constant value $\Phi = 1688 \text{ W}$. For the heat distribution on the friction ring, a constant applied pressure is assumed. The shape depends only on the sliding speed, which is a linear function of the radial position, and the sliding length, i.e. on the term $(1-S_{ratio}(r))$. The imposed and calculated heat fluxes are presented in Figure 6 and in Figure 7 with the relative error.

$$\Phi = \alpha * S_{pin} * P * v * \mu; \quad (10)$$

In Figure 6, the heat flux is presented on the mean friction radius during the test duration. This shows that the model captures the temporal evolution. Some errors appear with abrupt heat flux variations and are partially induced by the temporal stabilisation. The gap rapidly decreases and the error becomes less than 5% after 1 s. Regarding the radial distribution illustrated by heat fluxes at time $t=30 \text{ s}$ in Figure 7, the most significant errors are close to the friction ring edges where

the error can reach 40%. This can be explained by the low intensity of the dissipated power compared to the neighbouring positions on the friction ring. At the other locations, the error is always less than 5%. These results are obtained for $\beta = 2 \times 10^{-8}$. Tests have been performed for values of β between 1×10^{-7} and 1×10^{-9} . Below 1×10^{-8} , strong and non-physical disturbances appear in the estimated heat fluxes. From 1×10^{-8} to 3×10^{-8} , their shapes and intensities are close to the established values. For $\beta > 3 \times 10^{-8}$, the shape of the response becomes strongly smoothed. The errors are always more and more important between estimated and imposed heat fluxes on the edge of the friction ring. According to this analysis, the optimum value of β is 1.2×10^{-8} , but a value of 2×10^{-8} will be used because it allows the reduction of the disturbances caused by the data noise.

3. Experiments

The temperature data are obtained from tests performed on the High Speed Tribometer designed to reproduce braking conditions at a reduced scale. An adapted telemetry system allows for obtaining the temperature measurement using a contact method inside the rotating part.

3.1. High Speed Tribometer

The High Speed Tribometer has been developed by the TEMPO laboratory [27] to reproduce severe thermomechanical friction conditions. This device is designed on a Siemens MT1 high-speed machining system. The braking conditions are reproduced using a pin-on-disc configuration. For this friction disc diameter, the tribometer enables reaching a sliding speed until 50 m.s^{-1} on the mean friction radius (13000 rpm).

The disc is fixed on a HSK63 chuck with two zircon rings (Figure 8) with a low thermal conductivity (supplier : $k_{zirc}=1.6 \text{ W.m}^{-1}.\text{K}^{-1}$). These rings bring a thermal insulation from the other parts and allow the reproduction of a symmetrical heat flow at the half thickness of a full-scale disc. The broach can move on three translational axes and one rotational axis. A telemetry

device is adapted for use on the chuck to measure the temperature on the rotating part as described below.

The pin is 20 mm in thickness and is fixed on a rigid square. This is applied against the rotating disc by moving the broach in the normal direction until the researched initial contact pressure is achieved. Normal and tangential loads are measured with a 3D piezoelectric stress sensor (KISTLER). In this configuration, the HST can work up to 10 kN in the normal direction and 5 kN in the tangential direction. On the pin side, the temperature is measured using a K-type thermocouple inserted 1 mm under the pin contact surface. The sensor is fixed with a cement paste providing thermal properties close to the resin, which limits the heat flow perturbation induced by the hole.

3.2. Reduced scale rule

The disc and the pin are dimensioned so as to consider the reduced scale rule given by Sanders [28]. The friction surface ratio between the full scale $\frac{S_p}{S_D}$ and the reduced scale $\frac{S_p}{S_d}$ must be conserved (see Figure 9). This allows obtaining the same energy dissipation per unit area for a given sliding speed, normal pressure and friction coefficient. Regarding Roussette's work [29], the heat repartition between the pin and the disc is also conserved. The disc thickness is chosen to represent the half-full scale disc thickness. For commonly used ventilated discs, one side is approximately 10 mm in thickness. When using the pin on disc configuration, the heat is only dissipated on one side opposite to the braking system. For the full-scale brakes, the heat exchanges can be considered zero in the thickness direction, as heat fluxes coming from each side are equal. The insulation zircon ring placed on the disc back face plays the part of a thermal barrier and limits the heat conduction in the chuck.

3.3. Disc temperature measurements

Temperature measurements in the disc are performed with a telemetry device represented in Figure 8. This obtains data on the rotating part by inductive transfers. Eight sensors can be

connected on this system. Each sensor is connected to a amplifier module and the signals are transmitted to a multiplexer component. The complex signal is then recovered by an external part and each sensor data is finally conditioned to ± 5 V . To adapt the telemetry device, the friction disc has to be thermally insulated to avoid modules heating. The components do not tolerate a temperature above 80 °C during measurement.

The sensors are welded in the holes by capacitive discharge as described in Guillot's work [30]. The holes are 0.8 mm in diameter and are obtained by an electrical discharge machining. The thermocouple conductors are 0.1 mm in diameter to achieve a short response time (approximately 1 ms).

3.4. Tested conditions

The materials used in the experiments are similar to brake pads and disc. The pin samples are self-manufactured are made from pure commercial phenolic resin. An unreinforced material is chosen as the resin friction behaviour is simultaneously studied [31]. Cylindrical pieces are obtained by heating for 15 min at 150 °C with a normal pressure of 5 MPa. Compressed parts are initially 30 mm in diameter and are reduced to the dimensions with respect to the reduced scale rule.

Several pressure and sliding speed conditions are tested to evaluate their influence on the shape and the intensity of the generated heat fluxes. Regarding the initial normal load conditions, the tribological tests are performed at 0.35 MPa and 1.2 MPa. These pressures correspond to common and emergency braking pressure. Three sliding speeds are experimentally reproduced for the broach rotary speed of 1000, 2000 and 4000 rpm. These speeds correspond to 3.75, 7.5 and 15 $\text{m}\cdot\text{s}^{-1}$ at the mean friction radius. These sliding speeds are met on a full-scale disc for a saloon car cruising at 35, 70 and 140 $\text{km}\cdot\text{h}^{-1}$, respectively. For example, the data obtained for a test at 2000 rpm and 1.2 MPa are illustrated in Figure 5. The thermocouples and stress sensors enable simultaneously the acquisition of the temperature data inside the pin and disc, the mean pressure and the

friction coefficient evolution. It is acknowledged that the friction behaviour is highly dependent on the contact temperature. This value and the generated heat fluxes at the disc side are calculated using an inverse numerical method.

The heat transfer and the temperature field occurring in a disc during braking conditions can be calculated from temperature measurements performed at well-defined locations. Their numerical identification is possible provided that the thermal phenomena are well modelled. By knowing the other boundary conditions, it is possible to identify the heat fluxes generated on the disc friction ring with the inverse heat conduction method. The function specification method introduced by Beck [20] is used in this work and allows for the sequential estimation of the thermal conditions by minimising an error function between the numerical and experimental temperature values at the thermocouple locations.

4. Results

Regarding the pressure and the sliding speed conditions reproduced experimentally, some differences are observed in the heat flux distribution on the disc friction ring. The identification of the boundary conditions are illustrated for three chosen cases. In the Figure 11 are showed the results obtained for a mean normal pressure $P=1.2$ MPa and a sliding speed $v=3.75$ m.s⁻¹. On the left side, the temperatures measured in the disc are plotted for three radial positions $r=28$ mm, 36 mm and 44 mm, which is one millimetre under the contact surface. The calculated surface temperature is only shown for $r=36$ mm for visibility convenience. A temperature gradient is observed along the radial direction, and the maximum value is measured at the mean friction radius ($r=36$ mm) for the whole braking duration. However, a small temperature difference is observed between the surface and the sensor location at $r=36$ mm. This does not reach more than 5 °C during the test. On the right side, the identified heat fluxes calculated with the inverse algorithm are plotted. Values are presented for five radial positions along the contact surface : $r=28$ mm, 32 mm, 36 mm, 40 mm and 44 mm. The same presentation of temperature measurements and calculated heat fluxes is used for the other experimental cases.

In the Figure 11, the heat flux values are somewhat disturbed. This can be explained by the mean

normal pressure variation during the test as observed in the Figure 7. The experimental data noise must induce some non-physical variations when using the inverse model responses as well. In spite of the constant pressure and sliding speed conditions, a rapid decrease is also observed in all the identified boundary conditions at $t=40$ s . This is due to the friction coefficient loss induced by the fading phenomenon at elevated surface temperatures. Here, this behaviour is approximately observed at surface temperature 160-180°C.

Regarding the radial distribution, heat flux intensities are higher on the mean friction radius and tend to decrease with the distance from this position. This decrease can be explained by a larger surface ratio rubbing by the pin close to this location compared to the edges of the friction ring. Comparing the positions $r=28$ mm and $r=44$ mm, the heat generation is more important on the second position. The surface ratios are similar for these locations but the sliding speed increases with the distance from the disc centre. An increase in the energy dissipation for the same surface ratio is then consistent.

In the Figure 12, the temperature data and the heat fluxes for a test with a mean normal pressure of 1.2 MPa and a sliding speed of 15 m.s^{-1} are shown. For the sensor measurements, the temperature gradient becomes higher than in the previous case. The difference is also more important regarding the thickness direction at $r=36$ mm and can reach 25° between the surface and one millimetre under this position. Regarding the heat fluxes, the estimated values show that the heat generation tends to be localised at the mean friction radius. The ratio between the heat fluxes on the mean friction radius and on the friction ring edges becomes also larger with the increase in the sliding speed. The test duration is much shorter as the dissipated power is approximately four times more important. Regarding the disturbances in the heat fluxes, these are less important than in the previous case. As the temperature increases more rapidly, the inverse method solution is less affected by the data noise.

For the same sliding speed conditions (15 m.s^{-1}) with a pressure of 0.35 MPa, the results show that a lower normal load leads to a reduction in the heat generation localisation. As seen in Figure 13, there are little differences along the radial and the thickness directions for the temperature data.

This can be observed on the identified boundary conditions. For this last case, the decrease of the dissipated heat is also observed with a decrease in the friction coefficient.

These results show that the mean normal pressure and the sliding speed seem to have an influence on the distribution of the heat generated. On the disc friction ring, for all the experimental cases, a localisation on the mean friction radius has been observed for a high braking pressure ($P=1.2$ MPa) compared to a common braking pressure ($P=0.35$ MPa). In addition to the increase in the sliding speed, there seems to be higher induced temperature gradients between the radial positions on the friction ring. This may be responsible for more heat dissipation at the mean radius than at the friction ring edges as well.

5. Conclusion

In sliding contacts, the thermal conditions often have a significant influence on the tribological and wear behaviours. In braking systems, a better knowledge about the heat transfer and the temperature field in the disc is needed to understand and predict the fading phenomenon and the wear of the components. The heat generation on the disc is studied in this work from an inverse heat conduction model. The heat fluxes are calculated using an axisymmetric model to get the radial repartition with the function specification method. The experimental data are obtained from tests performed using a pin on disc configuration. The High Speed Tribometer reproduces braking conditions at a reduced scale. Temperature measurements on the rotating part are obtained with a telemetry device. Experimental tests are performed using a phenolic resin pin against low carbon steel disc for different automotive braking conditions. The calculated heat fluxes are consistent with the friction power that is thermally dissipated. An influence of the mean normal pressure and the sliding speed is observed over the range reproduced experimentally. In the future, the temperature measured using the telemetry device and calculated using the inverse heat conduction method should be coupled with an infrared camera. Knowing the temperature field by calculation will allow to identify emissivity maps on the rubbing surfaces. Combining these techniques is interesting to understand how the surface emissivity varies with the temperature and the surface

roughness evolution during a braking application. A supplementary temperature measurement in the pin is performed to simultaneously calculate the heat flux entering in the fixed part [32]. These results show that there is a non-negligible temperature gap between the disc and the pin surface. The thermal barrier appears with the presence of the surface asperities, the flow of worn particles and the bodies relative motion [33]. A pin-disc linked model is now developed to simultaneously determine the generated heat flux Φ_g , the heat repartition coefficient α and the dynamic thermal conductance h_c using an inverse technique.

Acknowledgements

This research has been supported by International Campus on Safety and Intermodality in Transportation, the Nord-Pas-de-Calais Region, the European Community, the Regional Delegation for Research and Technology, the Ministry of Higher Education and Research and the Carnot Arts Institute. The authors gratefully acknowledge the support of these institutions.

References

- [1] M. Eriksson, S. Jacobson, Tribological surfaces of organic brake pads, *Tribology International* 33 (2000) 817-827.
- [2] J. Bijwe, Nidhi, N. Majumdar, B. Satapathy, Influence of modified phenolic resins on the fade and recovery behavior of friction materials, *Wear* 259 (2005) 1068-1078.
- [3] B. Watel, S. Harmand, B. Desmet, Experimental validation of the feasibility of the brake disk equipped with a heat-pipe cooling, *Entropie* 191 (1995) 25-33.
- [4] B. Watel, S. Harmand, B. Desmet, Influence of flow velocity and fin spacing on the forced convective heat transfer from an Annular-Finned tube, *JSME international journal. Ser. B, Fluids and thermal engineering* 42 (1999) 56-64.
- [5] B. Watel, S. Harmand, B. Desmet, Etude de faisabilité du refroidissement d'un disque de frein équipé d'un caloduc, *Entropie* 187 (1994) 25-37.
- [6] J. Denape, N. Laraqi, Aspect thermique du frottement: mise en évidence expérimentale et éléments de modélisation, *Mécanique & Industries* 1 (2000) 563-579.
- [7] A. Anderson, Hot spotting in automotive friction systems, *Wear* 135 (1990) 319-337.
- [8] H. Blok, The flash temperature concept, *Wear* 6 (1963) 483-494.
- [9] J. Greenwood, An interpolation formula for flash temperatures, *Wear* 150 (1991) 153-158.

- [10] J. Barber, Thermoelastic instabilities in the sliding of conforming solids, *Proceedings of the Royal Society of London. Series A, Mathematical and Physical Sciences* 312 (1969) 381-394.
- [11] S. Panier, An experimental investigation of hot spots in railway disc brakes, *Wear* 256 (2004) 764-773.
- [12] P. Dufrenoy, G. Bodovillé, G. Degallaix, Damage mechanism of brake discs under thermomechanical loading, in: IXth Int. Conf. on Temperature-fatigue interaction (SF2M-ESIS Conference).
- [13] P. Ducrocq, F. Arpin, E. Markiewicz, S. Harmand, P. Drazetic, Estimation de la vitesse de déformation lors d'un choc par thermographie infrarouge *Mécanique industrielle et matériaux* (1996) 92-94.
- [14] J. Thevenet, M. Siroux, B. Desmet, Measurements of brake disc surface temperature and emissivity by two-color pyrometry, *Applied Thermal Engineering* 30 (2010) 753-759.
- [15] H. Kasem, J. Thevenet, X. Boidin, M. Siroux, P. Dufrenoy, B. Desmet, Y. Desplanques, An emissivity-corrected method for the accurate radiometric measurement of transient surface temperatures during braking, *Tribology International* 43 (2010) 1823-1830.
- [16] M. Siroux, H. Kasem, J. Thevenet, B. Desmet, P. Dufrenoy, Local temperatures evaluation on the pin-disc interface using infrared metrology, *International Journal of Thermal Sciences* 50 (2011) 486-492.
- [17] M. Siroux, A. Cristolbulthe, Y. Desplanques, B. Desmet, G. Degallaix, Thermal analysis of periodic sliding contact on a braking tribometer, *Applied Thermal Engineering* 28 (2008) 2194-2202.
- [18] N. Laraqi, N. Alilat, J. G. d. Maria, A. Baïri, Temperature and division of heat in a pin-on-disc frictional device-Exact analytical solution, *Wear* 266 (2009) 765-770.
- [19] Y. Yang, W. Chen, A nonlinear inverse problem in estimating the heat flux of the disc in a disc brake system, *Applied Thermal Engineering* 31 (2011) 2439-2448.
- [20] J. Beck, B. Blackwell, *Inverse heat conduction : ill-posed problems*, Wiley, New York, 1985.
- [21] B. Bourouga, Les aspects théoriques régissant l'instrumentation d'un capteur thermique pariétal à faible inertie, *International Journal of Thermal Sciences* 39 (2000) 96-109.
- [22] M. Siroux, S. Harmand, B. Desmet, Experimental study using infrared thermography on the convective heat transfer of a TGV brake disk in the actual environment, *Optical Engineering* 41 (2002) 1558.
- [23] H. Boyer, T. Gall, *Metals Handbook*, american society for metals edition, 1985.
- [24] K. Dowding, J. Beck, B. Blackwell, J. Hayes, A. Ulbrich, Estimation of thermal properties and surface heat flux in carbon-carbon composite, *Journal of Thermophysics and Heat Transfer* 9 (1995) 345-351.
- [25] J. Beck, B. Blackwell, A. Haji-Sheikh, Comparison of some inverse heat conduction methods using experimental data, *International Journal of Heat and Mass Transfer* 39 (1996) 3649-3657.
- [26] G. Blanc, M. Raynaud, T. Chau, A guide for the use of the function specification method for 2D inverse heat conduction problems, *Revue Générale de Thermique* 37 (1998) 17-30.
- [27] D. Meresse, Thermomechanical approach in high speed tribology - Braking application, Ph.D. thesis, Valenciennes, 2011. Manuscript in french.

- [28] P. Sanders, A reduced-scale brake dynamometer for friction characterization, *Tribology International* 34 (2001) 609–615.
- [29] O. Roussette, Y. Desplanques, G. Degallaix, Thermal representativity of tribological reduced-scale testing, *Comptes Rendus Mecanique* 331 (2003) 343-349.
- [30] E. Guillot, Etude expérimentale des transferts de chaleur à une interface pièce - outil de coupe, Ph.D. thesis, Université de Nantes, 2009.
- [31] D. Meresse, M. Watremez, M. Siroux, L. Dubar, S. Harmand, Friction and wear mechanisms study on a newly developed high speed tribometer, *AIP Conference Proceedings (ESAFORM2011)* 1353 (2011) 1759–1764.
- [32] D. Meresse, M. Siroux, M. Watremez, S. Harmand, L. Dubar, Thermal study of pin on disc sliding contact in automotive braking conditions, in: *JEF2010, 6th European Conference on Braking*.
- [33] N. Laraqi, Temperature and thermal resistance in frictional devices, *Applied Thermal Engineering* 24 (2004) 2567-2581.

Nomenclature

a	Thermal diffusivity	$\text{m}^2.\text{s}^{-1}$	δt	Time increment	s
C_p	Specific heat	$\text{J}.\text{kg}^{-1}.\text{K}^{-1}$	ϵ	Emissivity	
h	Convective coefficient	$\text{W}.\text{m}^{-2}.\text{K}^{-1}$	ν	kinematic viscosity	$\text{m}^2.\text{s}^{-1}$
k	Thermal conductivity	$\text{W}.\text{m}^{-1}.\text{K}^{-1}$	Φ	Heat flux	W
J	Functional to minimize		φ	Heat flux intensity	$\text{W}.\text{m}^{-2}$
M	Number of unknown heat fluxes		μ	Friction coefficient	
N	Number of sensors		ω	Rotary velocity	rpm
nft	Number of future time steps		ρ	Material density	$\text{kg}.\text{m}^{-3}$
P	Mean normal pressure	Pa	τ	Representative rate	
Re	Reynolds number		Subscripts		
r	Radial position	m	d	Disc side	
T	Calculated temperature	$^{\circ}\text{C}$	ext	Outer disc radius	
T_{∞}	External temperature	$^{\circ}\text{C}$	fext	Maximum friction ring radius	
t	Time	s	fint	Minimum friction ring radius	
v	Sliding speed	$\text{m}.\text{s}^{-1}$	i	sensor position	
X	Sensitivity coefficient	$\text{K}.\text{W}^{-1}.\text{m}^2$	ii	unknown heat flux position	
Y	Measured temperature	K or $^{\circ}\text{C}$	insu	Insulation radius	
z	Thickness position	m	int	Inner disc radius	
Greek letters			p	Pin/Pad side	
α	Heat flux partition coefficient		ratio	Cooled surface ratio	
β	Spatial regularisation parameter		zirc	Zircon	

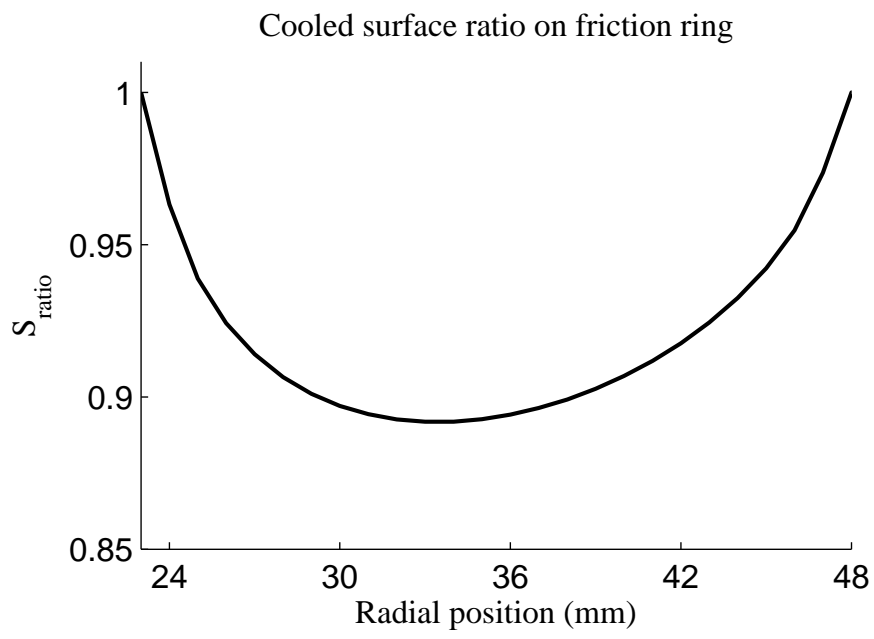


Figure 2: Friction ring cooled surface ratio

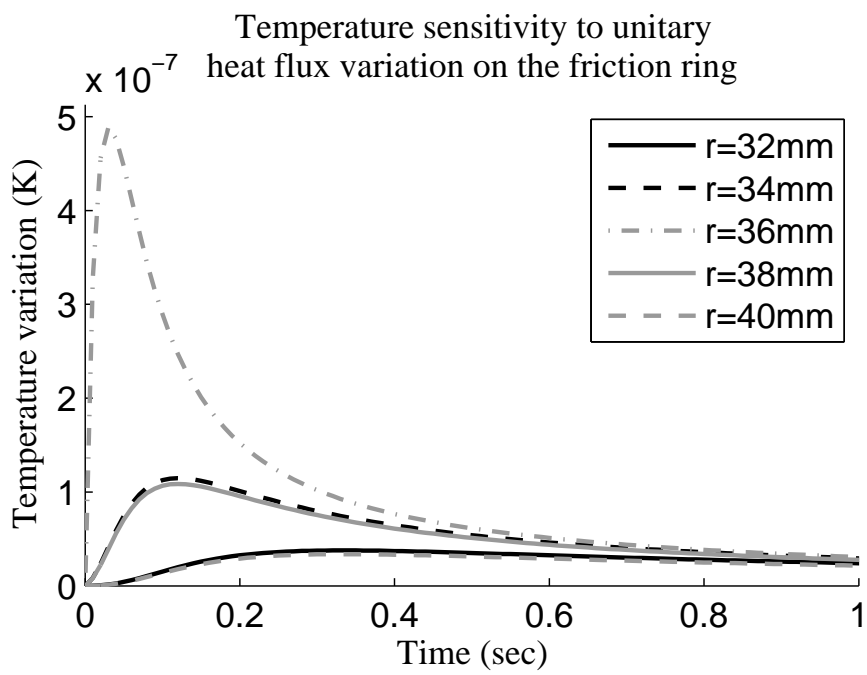


Figure 3: Sensibility analysis

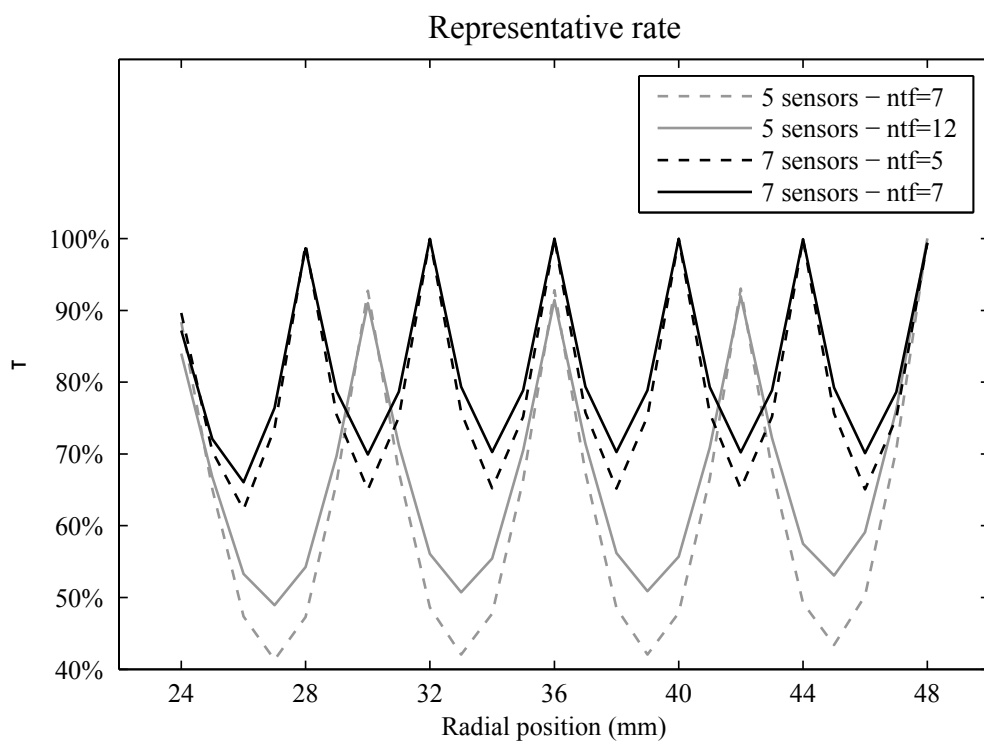


Figure 4: Rate of representation τ

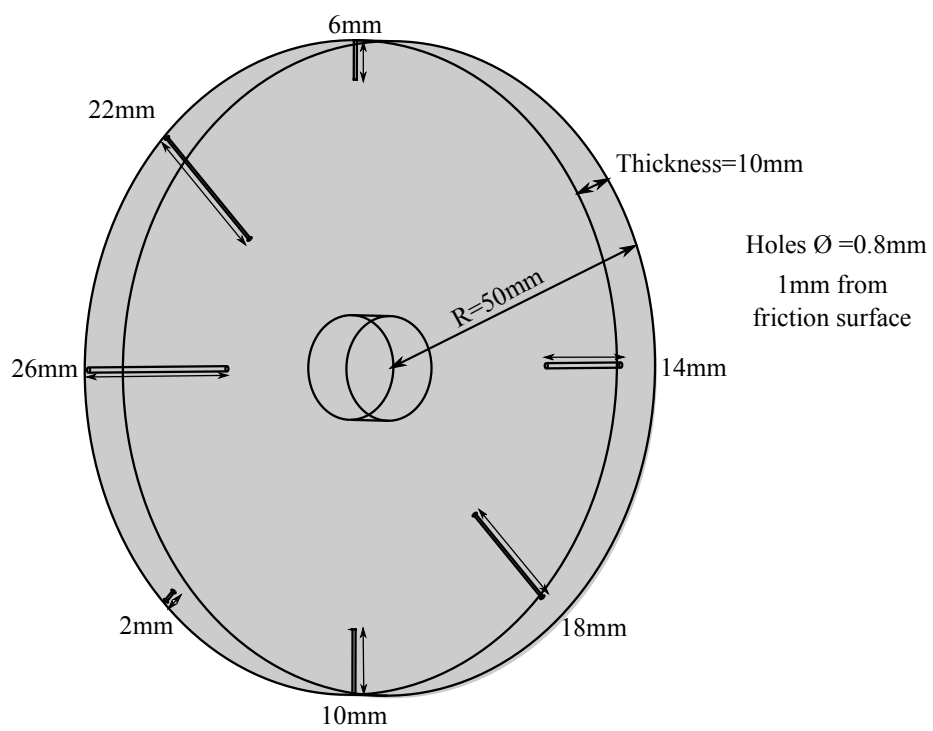


Figure 5: Disc thermocouples positions

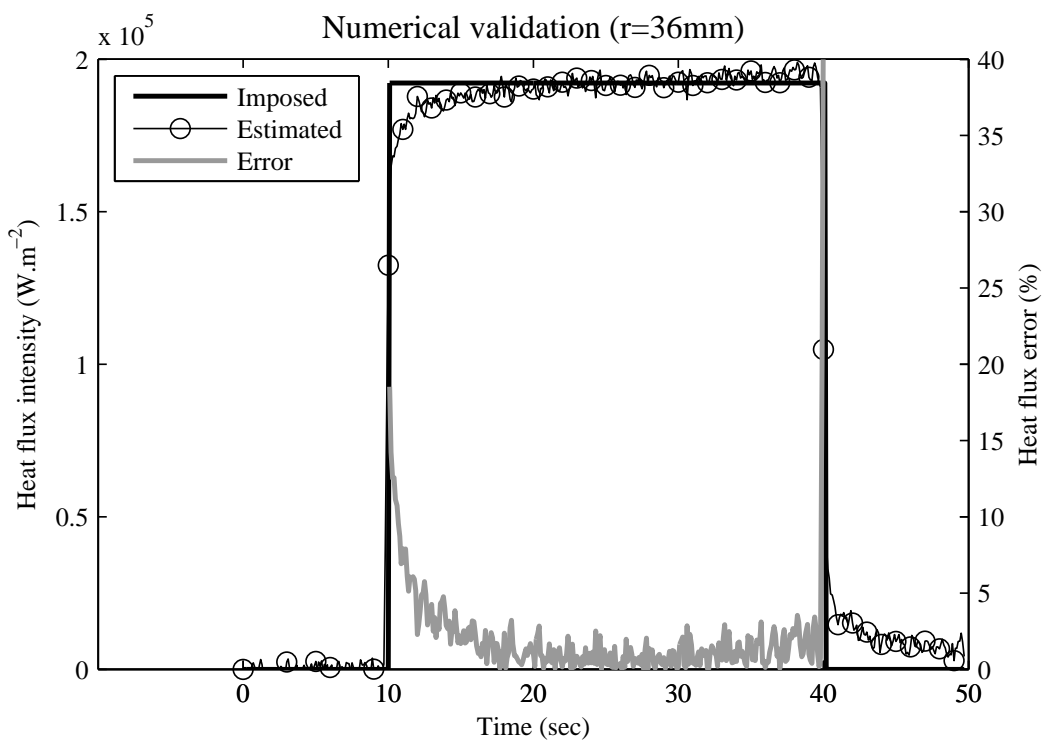


Figure 6: Numerical validation : comparison with time

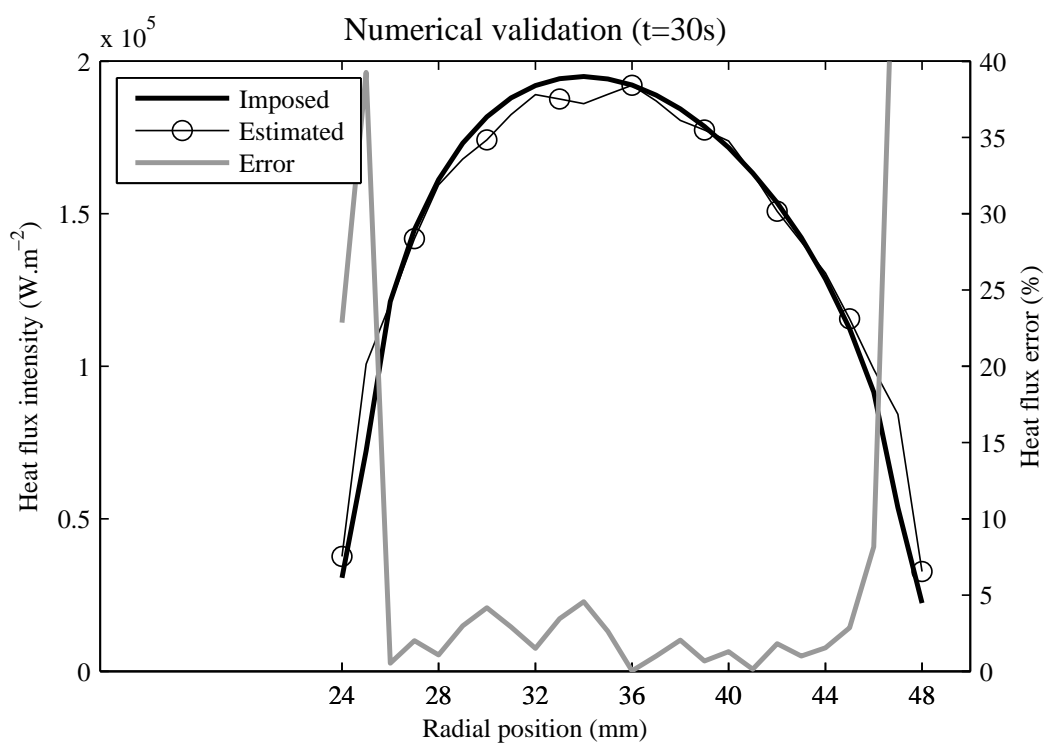


Figure 7: Numerical validation : comparison along the radial positions

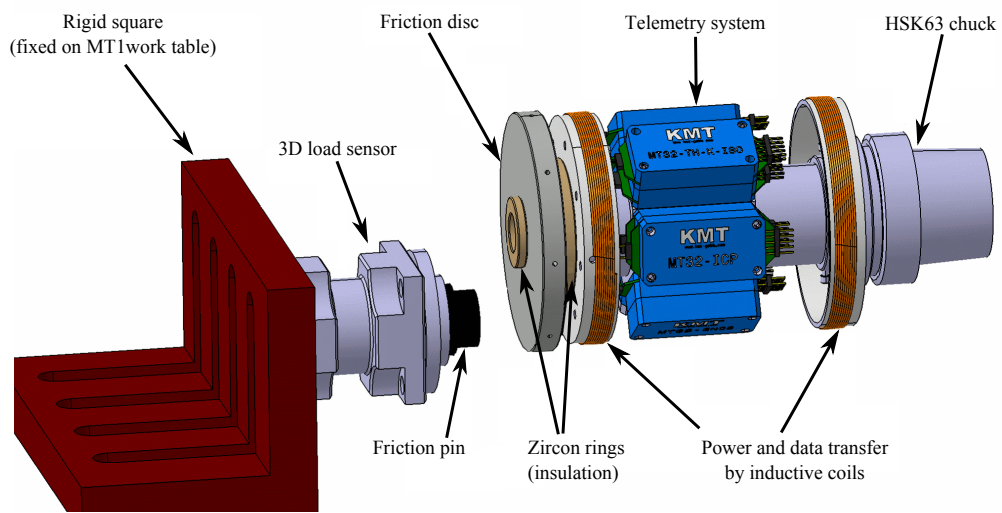


Figure 8: High Speed Tribometer

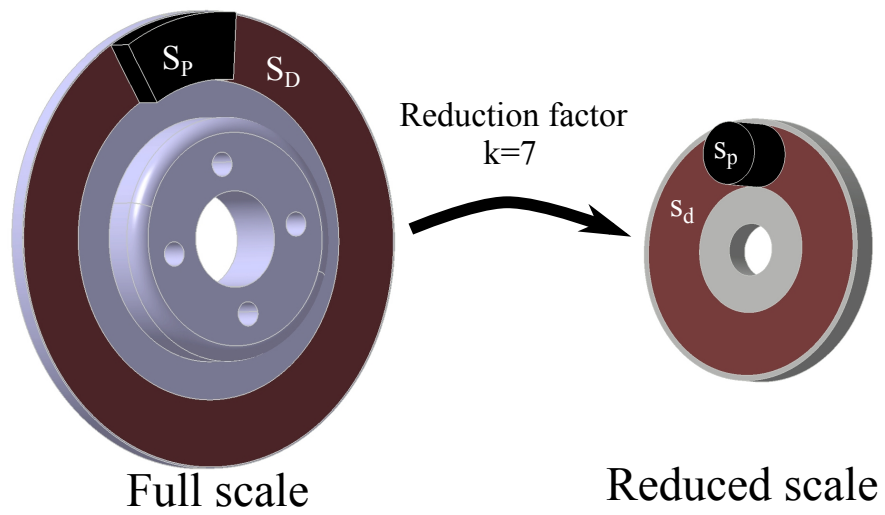


Figure 9: Reduced scale rule

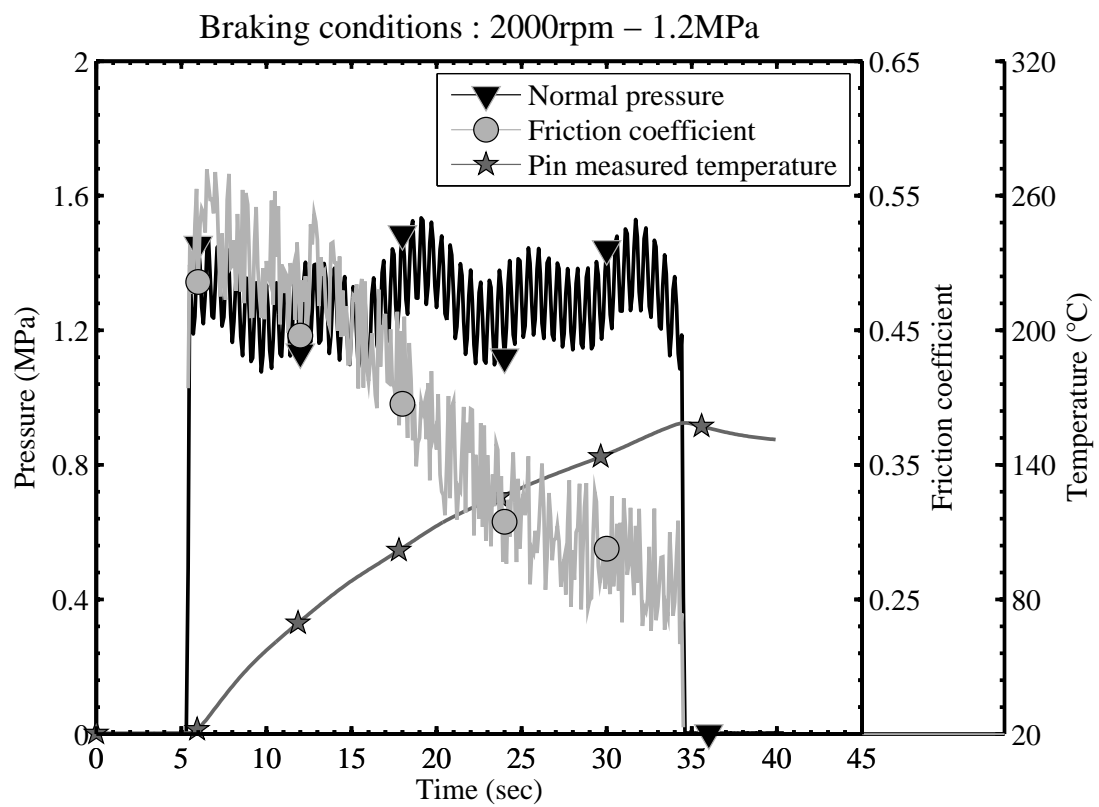


Figure 10: Pin temperature and loads - 2000 rpm - 1.2 MPa

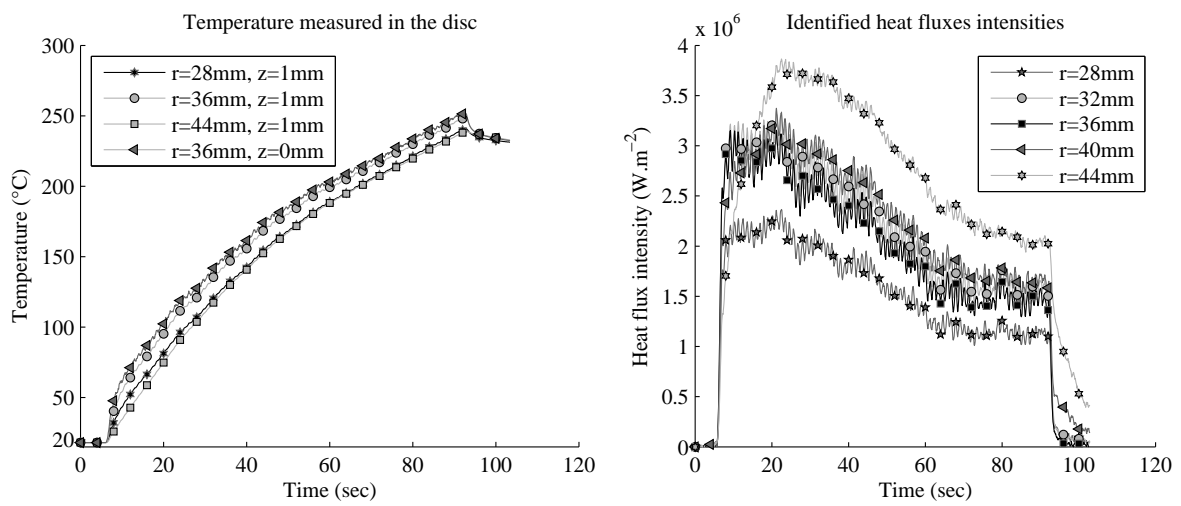


Figure 11: Measured temperatures and identified heat fluxes - $v=3.75 \text{ m}\cdot\text{s}^{-1}$ - $P=1.2 \text{ MPa}$

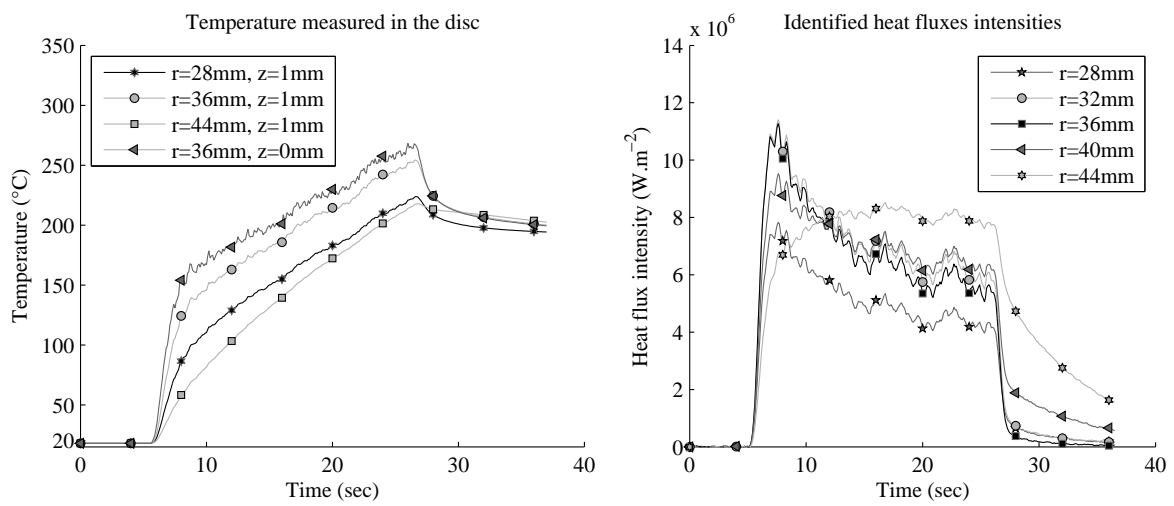


Figure 12: Measured temperatures and identified heat fluxes - $v=15 \text{ m.s}^{-1}$ - $P=1.2 \text{ MPa}$

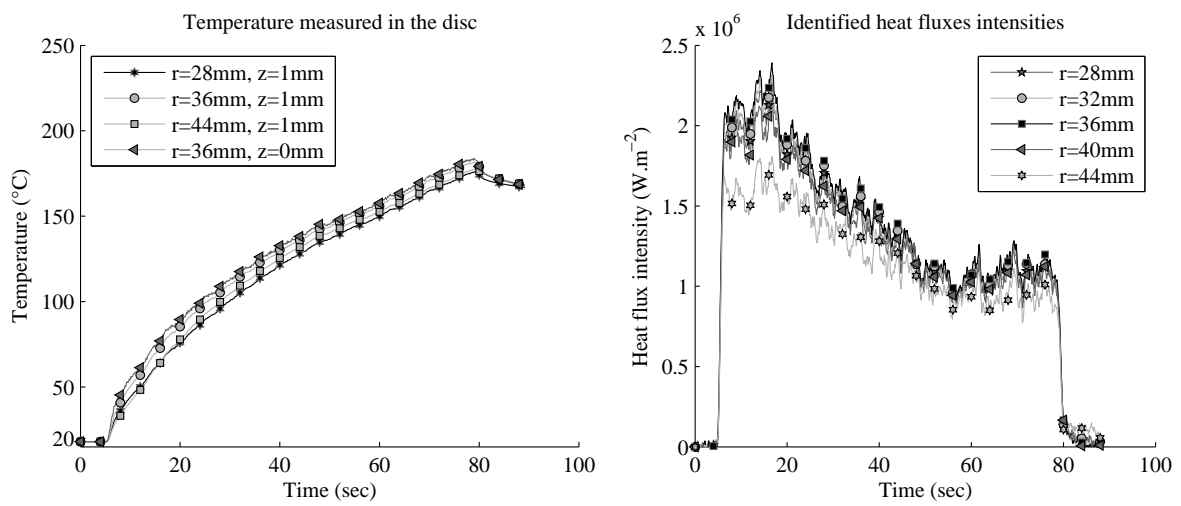


Figure 13: Measured temperatures and identified heat fluxes - $v=15 \text{ m.s}^{-1}$ - $P=0.35 \text{ MPa}$